Clutter Noise Reduction in B-Mode Image Through Mapping and Clustering Signal Energy for Better Cyst Classification

Asraf Mohamed Moubark, Sevan Harput, David M. J. Cowell and Steven Freear
Ultrasound Group, School of Electronic and Electrical Engineering, University of Leeds, UK.
E-mail: elamm@leeds.ac.uk and S.Freear@leeds.ac.uk

***Abstract*—Improving the ultrasound image contrast ratio (CR) and contrast to noise ratio (CNR) has many clinical advantages. Breast cancer detection is one example. Anechoic cysts which fill with clutter noise can be easily misinterpreted and classified as malignant lesions instead of benign. Beamforming techniques contribute to off-axis side lobes and clutter. These two side effects inherent in beamforming are undesirable since they will degrade the image quality by lowering the image CR and CNR. To overcome this issue a new post-processing technique known as contrast enhanced delay and sum (CEDAS) is proposed. Here the energy of every envelope signals are calculated, mapped, and clustered in order to identify the cyst and clutter location. CEDAS reduce clutter inside the cyst by attenuating it from envelope signals before the new B-Mode image is formed. With CEDAS, the image CR and CNR improved by average 12 dB and 1.1 dB respectively for cysts size 2 mm to 6 mm and imaging depth from 40 mm to 80 mm.**

I. Introduction

Clutter is a type of noise artefact in ultrasound images that often obscures anechoic regions such as cysts and blood vessels. This complicates and limits measurement of the cyst size and other anatomical measurements such as blood vessel and urine-filled bladders [1]. Clutter noise not only reduces the B-Mode image contrast but at the same time limits the depth at which diagnostic information can be obtained [2] [3]. A few main sources for clutter noise are reverberation, scattering from off axis and random acoustic noise [4]. Much work has been carried out to increase the image contrast ratio (CR) by eliminating or reducing the clutter noise effect. However not all manage to improve the B-Mode image CR together with contrast to noise ration (CNR). Work carried out by [5] manage to improve the image CR but not the CNR. But as a result of losing the image CNR values, the dynamic range has been increased by up to 100 dB. Increasing the dynamic range eventually decreases the image CR by returning the removed or reduced clutter noise inside the cyst. Thus a new signal post-processing technique known as CEDAS is proposed in this paper. Here, the clutter noise inside the cyst is attenuated, CR increased and CNR maintained by mapping and clustering the energy level of the envelope signal.

II. Methods

The first step in identifying the location of a cyst and eliminating the clutter inside it starts with calculating the energy of the envelope signal for each of the image lines using the windowing technique [6]. Mapping the envelope signal into energy through the windowing process helps to classify and differentiate from the speckle destructive region and the clutter inside the cyst. Classifying clutter inside the cyst with radio frequency (RF) or envelope signals is not feasible. This is because the speckle destructive region produces the same values as the clutter inside cyst.The energy of the envelope signal, G_i calculated from a small segment separately. According to rectangular window size, *N*, G_i is given by following equation:

$$G_i = \sum_{j=0}^{N-1+k} |X_{j+k}|^2 \tag{1}$$

$$i = 1, 2, ..., n; \qquad n = (m - N)/s; \qquad k = 0, s, 2s, ..., ns.$$

Where *X* is number of sample in envelope signal, *i* is number of windowing, *k* is the step increment from one window to another, *s* is an integer even number, *m* is the length of the envelope signal and finally *n* is total number of windowing. All small chunks of energy calculated for each window, G_i are merged so that it becomes one single energy line, E_l as given by

$$E_l = 20\log_{10}\{G_{i=1}(0:s), G_{i=2}(2s:3s), ... \\ ..., G_{i=n}((n-1)s:ns)\} \tag{2}$$

Where l represents the number of imaging lines. Next, before grouping or clustering the energy level into different groups, the transition of the energy level or change in the energy mean are determined. The main objective is to find the most significant changes in the energy level to identify hyperechoic, speckle and hypoechoic region. The highest levels of energy indicate a hyperechoic region. Medium levels of energy indicate speckle region while the lowest energies indicate cyst or hyperechoic regions. Optimal detection of change-points algorithm created by [7] have been used to find the points where the energy signal mean changes most significantly by specifying a minimum residual error improvement in the function. More detailed mathematical

works on finding abrupt points can be found in [7] [8]. All changing points, q_{ld} obtained for every energy line, E_l are contained in the following matrix,

$$Q_l = \begin{pmatrix} q_{11} & \cdots & q_{1c} \\ \vdots & \ddots & \vdots \\ q_{x1} & \cdots & q_{xc} \end{pmatrix} \tag{3}$$

$$q_{ld} \in E_l; \qquad d = 1, 2, ..., c.$$

Where the first horizontal direction in the matrix, $Q_{l=1}$ represents all changing points, $(q_{1_1}, q_{1_2}, ..., q_{1_c})$ in the first energy line, $E_{l=1}$ while c represents the total number of changing points.

Once the changing points on the energy signal level are identified for all the lines, they are next grouped or clustered into four different groups by using k-means clustering technique as given by [9]

$$J(a) = \sum_{a=1}^{p} \sum_{l=1}^{x} \parallel Q_l - v_a \parallel^2 \tag{4}$$

$$p < x$$

Where p is the number of clusters and v_a are the centroids for cluster a. The second lowest cluster, $J(a-1)$ was used as a threshold to determine the clutter present. The new envelope signal, $\grave{X}$ was formed for every image line according to the condition stated below

$$\grave{X} = \begin{cases} X, & Q_l \geq J(a-1) \\ \mathrm{X} \times 0.25, & Q_l < J(a-1) \end{cases} \tag{5}$$

New envelope signal formed, $\grave{X}$ is equal to former envelope signal, X if the changing points, Q_l is more than the data inside the second lowest cluster, $J(a-1)$ else X is attenuated by factor of 0.25 if the changing point, Q_l is lower than data inside the second lowest cluster, *J(a-1)*. The new envelope signals are converted into a log scale to form B-Mode image.

III. Simulation and Performance Evaluation

In order to evaluate the performance of the proposed method, Field II [10] simulations have been carried out on multiple cyst diameter sizes from 2 mm to 6 mm at different depths, between 40 to 80 mm. The simulation parameters are shown is Table 1. A B-mode image was formed with plane wave imaging (PWI) steered at a 0° angle. The window size, *N* used for the simulation was 64 and the increment size, *k* is 2. If the increment step is small, the overlapped region between the windows will be more and this will eventually produce smoother transition in the energy values calculated between the windows. The whole process of calculating the energy from the envelope signal is shown in Fig. 1(a). The variation of speckle formation that is produced from constructive and destructive interference of the scattering signal as can been seen in Fig. 1(b) are now becoming less as in Fig. 1(c).

TABLE I
Simulation Parameters

Parameters	Values
Speed of Sound, m/s	1540
Sampling Frequencies, MHz	160
Centre Frequencies, MHz	5
Bandwidth, %	100
No. of Elements	128
Elements Spacing	λ
Excitation Signal	Hanning Windowed 2 Cycles Sinusoidal

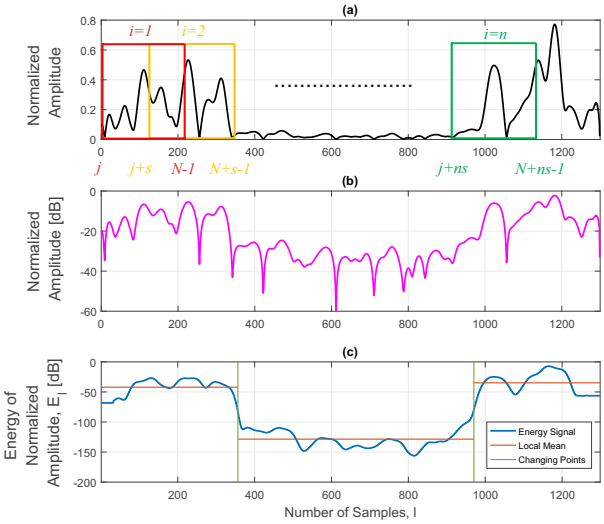

Fig. 1. (a) Energy calculated by applying the windowing technique on the envelope signal. (b) Envelope signal in dB scale. (c) Shows the energy values calculated from (a) mapped into single lines.

The energy changing points were sorted from minimum to maximum before they were clustered in order to have better visualisation on the cluster hierarchy. All four clusters are shown in Fig. 2 with their centroids points. Note that the clusters are not in order since k-means assigned centroid points randomly . Thus centroids points are sorted before each one of the cluster identified in order. The lowest clusters are considered as clutter regions and the preceding cluster group is used as the threshold level. In Fig. 2 data in cluster 1 ,red, was used as a threshold. In the case where only two changing points in the energy level are present, the clustering divided whole points into four groups where upper or the top two groups represent the same energy region and the lowest groups represent clutter.

IV. Performance Evaluation

In order to evaluate the final B-Mode images qualities formed with DAS and CEDAS techniques, two key performance indicator haven used. First the CR is used to express the

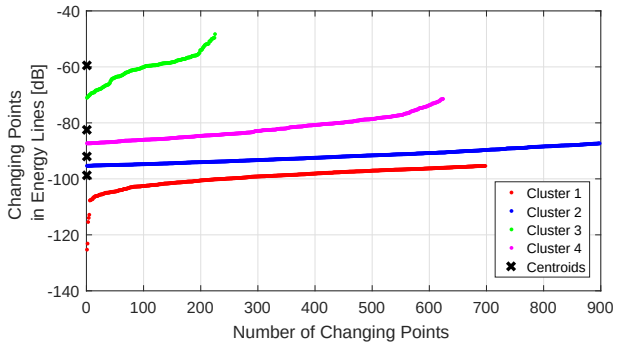

Fig. 2. Cluster assignment for changing points in the energy level.

detectability of the object contrast between region of interest (ROI) inside the cyst and its background. Second the CNR is used the measure the cyst contrast with speckle or noise variation inside and outside of the cyst [11]. High CNR value means cyst can be visualize easily and the acoustic noise standard deviation is small or more uniform. Both CR and CNR equation are given by

$$\text{CR(dB)} = 20\log_{10}\left(\frac{\mu_{cyst}}{\mu_{back}}\right) \tag{6}$$

$$\text{CNR(dB)} = 20\log_{10}\left(\frac{|\mu_{cyst} - \mu_{Back}|}{\sqrt{({\sigma_{cyst}}^2 + {\sigma_{Back}}^2)}}\right) \tag{7}$$

Where μ_{cyst} and μ_{Back} are means of image intensities inside and outside of the cyst respectively while ${\sigma_{cyst}}^2$ and ${\sigma_{Back}}^2$ are their variances. CR and CNR were calculated on the cysts at different depths on the B-Mode images produced by creating two different regions with the same dimensions. The first region is inside the cyst while the other region is located outside the cyst at the same depth. This is to ensure that the attenuation caused by frequency doesn't affect the measurements.

V. Results and Discussions

In this section, performance of both conventional DAS and CEDAS were evaluated qualitatively as shown in Fig. 3 and quantitatively as presented in graphical form in Fig 4. B-Mode image of conventional DAS as shown in Fig. 3(a) clearly shows that all ten cysts are effected by clutter noise. The noise level inside the cysts increase with depth. One of the reason for high noise level is due to low signal-to-noise ratio from PWI [12]. On the other hand, the proposed method, CEDAS as shown in Fig. 3(b) successfully detect and attenuated almost all clutter noise that is present inside those cysts.

These results are supported by the axial distance graph shown in Fig. 4(a) and the lateral distance graph as shown in Fig. 4(b). Both graphs show that clutter noise variations inside the cyst are attenuated.

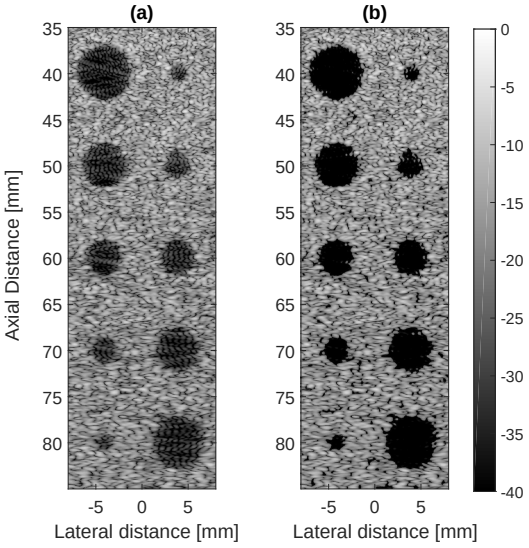

Fig. 3. B-Mode images for (a) DAS, (b) CEDAS.

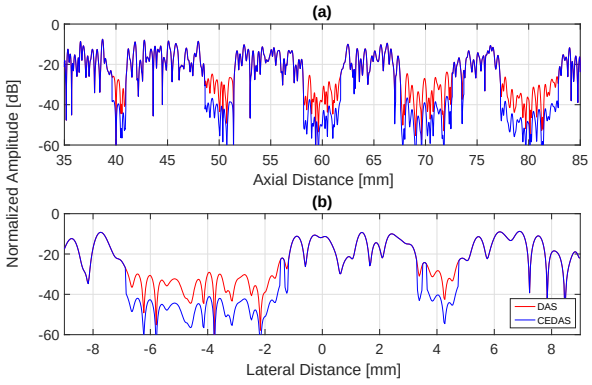

Fig. 4. (a) Axial Distance plotted from -4 mm, (b) Lateral Distance plotted from 40 mm location referring to Fig. 3.

As predicted, the CR for CEDAS out performed DAS. At a depth of 40 mm, the CR for DAS is -21 dB while for CEDAS is -33 dB. The CR difference between both techniques retained throughout the depth regarding the cyst sizes. In average, CR for CEDAS is 12 dB higher than DAS. Complete results presented in Fig. 5(a). At the same time, the CNR values for CEDAS also increases compared to DAS even though no changes are applied to the speckle formation outside the cyst. Initial hypothesis was made that the CNR values will be same in both techniques. However due to less noise variance inside the cyst for CEDAS compared to DAS, the CNR value also increase. At 40 mm depth the CNR values for CEDAS is 5 dB compared to 4.3 dB for DAS. CEDAS continuously produces better results compared to DAS by average 1.1 dB for all cyst size at all depth as shown in Fig. 5(b).

The ability for an object to be easily detected depends on the contrast. Since CEDAS enhanced the CR, the border of the cyst can be easily detected. Edge detection technique applied

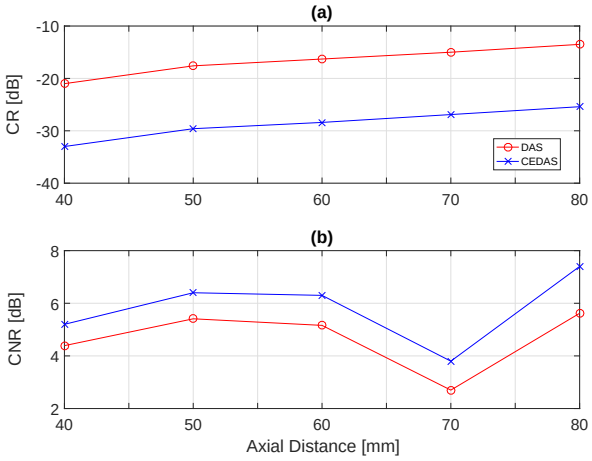

Fig. 5. (a) CR, (b) CNR for DAS and CEDAS.

on 6 mm diameter cyst located at 40 mm depth using Sobel methods with fudge factor of 0.3 is shown in Fig. 6. CEDAS able to trace the edge inside the cyst while DAS could not since the noise variation is high.

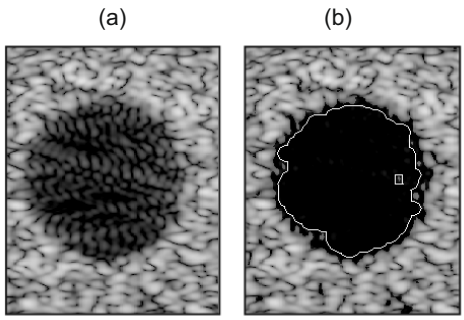

Fig. 6. Border detection using Sobel method on (a) DAS, (b) CEDAS.

A histogram is plotted for the number of amplitude occurrences on both B-Modes images as shown in Fig. 3(a) and (b). The histrogram as shown in Fig. 7 shows significant changes in the distribution of the amplitude. The speckle and strong reflective points which dominate higher amplitude portion shows more number of occurrence with CEDAS when compared to DAS. This is due to reduction or attenuation of clutter noise. Normalizing signal with less noise level eventually give rise to high value signal. Thus non-cyst region in Fig. 3(b) shows more prominent when compared with same region in Fig. 3(a). At the same time, it can be seen on the histogram that second smaller peaks appear on CEDAS amplitude distribution approximately at -57 dB. This portion represent clutter noise which have been brought down through attenuation process. Displaying the B-Mode image with 40 dB dynamic range eventually dimmed its appearance and increase the image CR and CNR. Area under the curves for both amplitude distribution is same.

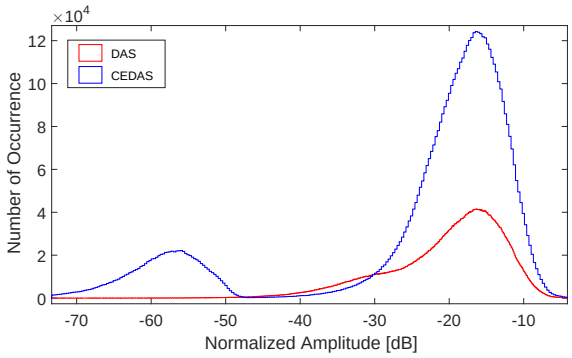

Fig. 7. Histogram for DAS and CEDAS normalized amplitude distribution.

VI. Conlusion

The proposed new technique, CEDAS has successfully demonstrated its ability to eliminate clutter inside the cysts with diameter of 6 mm to 2 mm from 40 mm to 80 mm depths. High CR and CNR is achieved without changing or modifying any formation of the B-Mode image. Edge detection on cyst border also improved with CEDAS. Since the idea is only implemented on PWI with DAS, future works will be carried out on compound PWI and other beam-forming techniques such as filtered delay and sum (FDMAS). Data from laboratory experiments on a multi-purpose phantom also will be used to test the workability of this new technique.

References

[1] M. A. Lediju, M. J. Pihl, J. J. Dahl, and G. E. Trahey, "Quantitative assessment of the magnitude, impact and spatial extent of ultrasonic clutter," *Ultrasonic imaging*, vol. 30, no. 3, pp. 151–168, 2008.

[2] S. Huber, M. Wagner, M. Medl, and H. Czembirek, "Real-time spatial compound imaging in breast ultrasound," *Ultrasound in medicine & biology*, vol. 28, no. 2, pp. 155–163, 2002.

[3] R. Entrekin, P. Jackson, J. Jago, and B. Porter, "Real time spatial compound imaging in breast ultrasound: technology and early clinical experience," *medicamundi*, vol. 43, no. 3, pp. 35–43, 1999.

[4] F. Tranquart, N. Grenier, V. Eder, and L. Pourcelot, "Clinical use of ultrasound tissue harmonic imaging," *Ultrasound in medicine & biology*, vol. 25, no. 6, pp. 889–894, 1999.

[5] S. A. Izadi, A. Mahloojifar, and B. M. Asl, "Weighted capon beamformer combined with coded excitation in ultrasound imaging," *Journal of Medical Ultrasonics*, vol. 42, no. 4, pp. 477–488, 2015.

[6] S. Nisar, O. U. Khan, and M. Tariq, "An efficient adaptive window size selection method for improving spectrogram visualization," *Computational Intelligence and Neuroscience*, vol. 2016, 2016.

[7] R. Killick, P. Fearnhead, and I. Eckley, "Optimal detection of change-points with a linear computational cost," *Journal of the American Statistical Association*, vol. 107, no. 500, pp. 1590–1598, 2012.

[8] M. Lavielle, "Using penalized contrasts for the change-point problem," *Signal processing*, vol. 85, no. 8, pp. 1501–1510, 2005.

[9] A. Likas, N. Vlassis, and J. J. Verbeek, "The global k-means clustering algorithm," *Pattern recognition*, vol. 36, no. 2, pp. 451–461, 2003.

[10] J. A. Jensen, "Users guide for the field ii program," *Technical University of Denmark*, vol. 2800, 2001.

[11] J. S. Ullom, M. Oelze, and J. R. Sanchez, "Ultrasound speckle reduction using coded excitation, frequency compounding, and postprocessing despeckling filters," in *2010 IEEE International Ultrasonics Symposium*. IEEE, 2010, pp. 2291–2294.

[12] A. M. Moubark, Z. Alomari, S. Harput, and S. Freear, "Comparison of spatial and temporal averaging on ultrafast imaging in presence of quantization errors," in *Ultrasonics Symposium (IUS), 2015 IEEE International*. IEEE, 2015, pp. 1–4.